Int. J. Electrochem. Sci., 15 **(2020)** 3646 – 3659, doi: 10.20964/2020.05.49

International Journal of
ELECTROCHEMICAL
SCIENCE
www.electrochemsci.org

Optimization of Machining Parameters and Electrochemical Corrosion Behavior of hardened Cr12MoV Mold Steel

Chen Guangjun[1,2,*], *Hou Shuai*[2], *Han Songxi*[2], *Wang Chuanliang*[3]

[1] School of Mechanical Engineering, Tianjin University of Technology and Education, Tianjin 300222, China
[2] School of Mechanical Engineering, Jiamusi University, Jiamusi 154007, China
[3] School of Mechanical Engineering, Shenyang Jianzhu University, Shenyang 110168, China
[*]E-mail: guangjunchen08@sina.com

Received: 11 December 2019 / *Accepted:* 20 February 2020 / *Published:* 10 April 2020

Corrosive environment can influence on hardened steel containing Cr12MoV dies during molding which lead to greatly reduce the service life of the molds. Therefore, it is important to investigate the influence of milling parameters on the corrosion resistance of the metal die surface. In this study, single factor cutting tests and electrochemical methods were used to study the effect of processing parameters on the corrosion resistance of Cr12MoV steel die used traditionally in injection molding of plastics. Polarization curve and impedance spectrum of the material was measured in mixed acid solutions under different processing parameters. ZSimpWin software was used to fit the impedance data and to analyze the corrosion resistance of the steel alloy die. The surface morphology after corrosion was observed under a scanning electron microscope (SEM), and elemental analysis was done to characterize the corrosion products. The corrosion resistance of the Cr12MoV die steel had a great correlation with the skewness and kurtosis of the surface morphology parameters. Skewness values closer to zero resulted in smaller kurtosis values and increased corrosion resistance of the machined surface during injection molding. Among different conditions, the change of cutting depth had little effect on the corrosion resistance of the material surface. However, the change in tool radius had a significant impact on the corrosion resistance of the workpiece. The SEM results revealed that the corrosion products were found to significantly accumulate on the surface of the workpiece which was in accordance with the electrochemical results.

Keywords: Electrochemical Corrosion, Milling Surface, Polarization Curve, Electrochemical impedance spectroscopy, Milling Parameters, Corrosion Morphology

1. INTRODUCTION

In order to improve the production efficiency of hardened steel mold used for injection molding of plastics, milling instead of grinding is often used, since the processed surface usually directly serves

as the final molding surface. However, during plastic molding, these metal molding surfaces are often eroded by corrosive gases such as hydrogen chloride and hydrogen fluoride that are traditionally formed from thermal decomposition of the plastics, thus greatly reducing the service life of the molds. Milling is a complex thermo-mechanical coupling process, different processing technologies have a great impact on the corrosion resistance of the machined surface [1-3]. Therefore, it is of great significance to study the influence of different processing parameters on the corrosion resistance of the machined surface of hardened steel and its alloys.

Currently, significant research has been done on improving the corrosion resistance of the workpieces. Zhang et al found that the corrosion rate of 316L stainless steel bellows was greatly reduced after surface-blackening treatment [4]. Junior et al. found that the corrosion resistance of stainless steel was significantly improved when processed with high pressure cooling and high cutting speed [5, 6]. Zhang et al. characterized the degree of corrosion in a metal surface using a corrosion damage area method and the corrosion depth. The study focused primarily on the corrosion resistance of milling surface of aluminum alloy and found that the corrosion resistance of the workpiece could be improved by improving the processing parameters [7]. Liptáková et al. showed that AISI316Ti stainless steel treated by shot peening had better corrosion resistance in chloride-containing environment [6, 8].

The above studies primarily focused on investigating the corrosion resistance of a workpiece surface to improve surface modifications, other studies focused on the influence of processing parameters on the corrosion resistance of metal surface [9-11]. While machining parameters are the most direct factors affecting the surface morphology, the corrosion resistance of samples does not necessarily increase with a decrease in the surface roughness [12], Wang used grey relational method in order to conclude that the corrosion resistance of the workpiece is closely related to the skewness and kurtosis of the machined surface [13, 14]. The main acid solution system used for acidification is mud acid, which consists of hydrofluoric (HF) acid and hydrochloric (HCl) acid [15]. In this study, single factor cutting tests and electrochemical methods were used to study the effect of processing parameters on the corrosion resistance of metal surface die used traditionally in injection molding of plastics. The corrosion mechanism of the workpiece surface is analyzed by introducing surface skewness and steepness, which can be a significant reference during production and processing. Solvent mixture containing 0.1 mol/L HF acid and 0.3 mol/L HCl acid was used as the electrolyte solution.

2. MATERIALS AND METHOD

Chemical compositions of Cr12MoV steel are shown in Table 1. The dimensions of the workpiece are 50mm * 30mm * 30mm, and the hardness of the workpiece after quenching is HRC56. The milling test was carried out on V950L type milling machine with a maximum speed of 10000 rpm and clamping angle of 15 degrees. CoroMill (Sandvik Coromant; Sandwich Wicken, Sweden) ball end finishing tool was selected and dry milling was adopted as the primary processing method. Three-dimensional (3-D) morphology parameters were measured with 3D optical surface profiler

NewViewTM 8000(ZYGO; Connecticut, America). The electrochemical corrosion test was carried out on Princeton VersaSTAT3 electrochemical workstation and JSM-7800F scanning electron microscope (SEM, JEOL; Tokyo, Japan) was used to observe the surface morphology of the corroded workpiece and energy dispersive spectrometer (EDS) analysis.

Table 1. The Chemical composition of Cr12MoV alloy (wt.%).

Cr	**C**	**V**	**Mn**	**Si**	**Mo**	**Cu**
11.00~12.50	1.45~1.70	0.15~0.30	≤0.40	≤0.40	0.4.~0.60	≤0.3

Single factor design was adopted to study the effects of cutting speed, feed rate, cutting depth, cutting row spacing and tool radius on the corrosion resistance of the workpiece surface. Table 2 shows the experimental design using these factors. After the milling test, the material was cut into small pieces (size: 15mm * 15mm * 8mm), cleaned and dried with absolute ethanol in an ultrasonicator (Elma; Konstanz, Germany). Optical surface profilometer (ZYGO; Connecticut, America) was used to measure the 3-D surface morphology before and after onset of corrosion on the workpiece. After the electrochemical corrosion, the solution on the metal surface was slowly buffered using tap water and dried with an air-blower.

Table 2. Cutting parameters for experimental design

Cutting speed v/(m·min^{-1})	Feed rate f/(mm·r^{-1})	Cutting depth a_p/(mm)	Row distances a_e/(mm)	Cutter radius r/(mm)
49	0.05	0.1	0.1	5
123	0.1	0.2	0.2	6
197	0.15	0.3	0.3	8
270	0.2	0.4	0.4	
344	0.25	0.5	0.5	

The electrochemical experiments were carried out using a home-made three-electrode system. The bottom surface of the workpiece cutting sample was polished with yarn paper. The copper wire was then welded to this bottom surface using a tin wire and the non-working surface was sealed with paraffin. An area of 1 square centimeter on the working surface was used as the “working electrode”. The auxiliary electrode was a platinum plate electrode with an area of 1 square centimeter, and a saturated calomel electrode (SCE) was used as the reference electrode. Solvent mixture containing 0.1 mol/L hydrofluoric acid and 0.3 mol/L hydrochloric acid was used as the electrolyte solution. The working electrodes were immersed in the solution for two minutes, and electrochemical impedance spectroscopy (EIS) was tested when the open circuit potential was basically stable. The amplitude of the excitation signal was 10 mv, and the measuring frequency ranged was from 10 000 to 0.01 HZ. The

scanning rate and sweep range of potentio-dynamic polarization curve were 0.5 mv/s, and -0.5-0.5 V, respectively. The data was acquired using Versa Studio software and the impedance data was fitted using ZSimpWin software.

3. RESULTS AND DISCUSSION

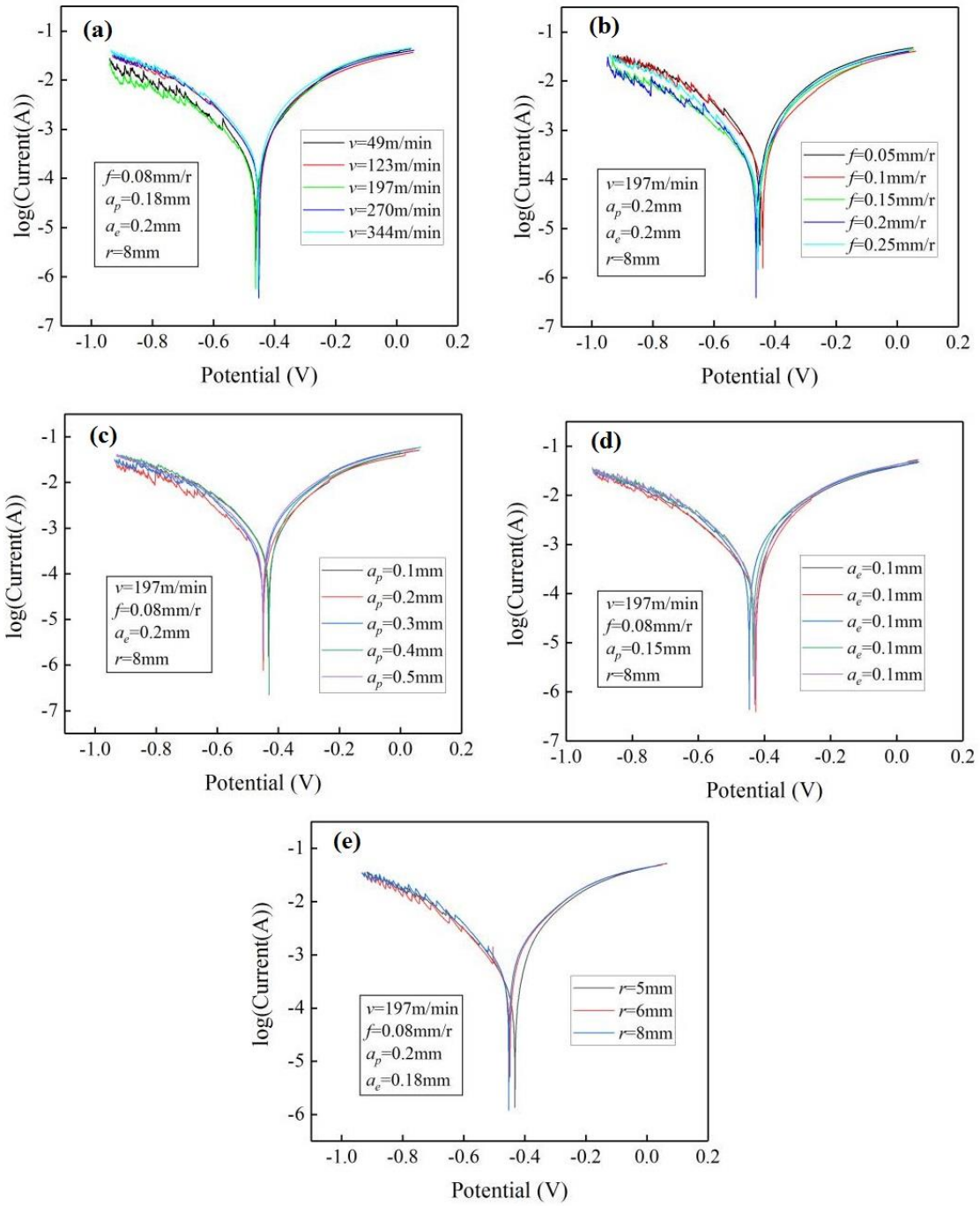

Figure 1. Polarization curves corresponding to different processing parameters (a) Cutting speed (b) Feed rate (c) Axial cutting depth (d) Row spacing (e) Tool Radius at scanning rate of 0.5 mv/s sweep range of -0.5 to 0.5 V

The polarization curves of the samples processed in the mixed acid solutions under different processing parameters are shown in Figure 1. As shown in Fig. 1, the sample processed under different parameters revealed different resistance of corrosion. Corrosion current density can be used to measure the rate of corrosion [16]. The smaller the corrosion current density indicate the higher corrosion resistance of the sample. The corrosion current density (I_{corr}) was obtained through tafel extrapolation of the polarization curve.

Surface skewness (S_{sk}) and kurtosis (S_{ku}) can be used to characterize the morphological properties of the surface which is related to the corrosion resistance of the samples [17]. S_{sk} can reflect the asymmetry of the surface-amplitude distribution. When S_{sk} is equal to 0, it means that the surface amplitude distribution is uniform and symmetrical, i.e., Gaussian in nature. However, as the S_{sk} is less than 0, it means that there are a significant number of deep valleys on the surface [18]. If S_{sk} is greater than 0, it means that there may be more bumps on the surface. The kurtosis reflects the sharpness of the surface peak in an amplitude distribution curve. When the profile amplitude distribution curve conforms with Gaussian distribution, the kurtosis value, S_{sk} was found to be about 3. Based on the Gaussian distribution curve, as the kurtosis value, S_{sk} increased over 3, the shape of the amplitude distribution curve was steep, indicating that there were more peaks on the surface. Once $S_{ku} < 3$, the curve of the amplitude distribution was wide and flat, which is called low peak curve [19].

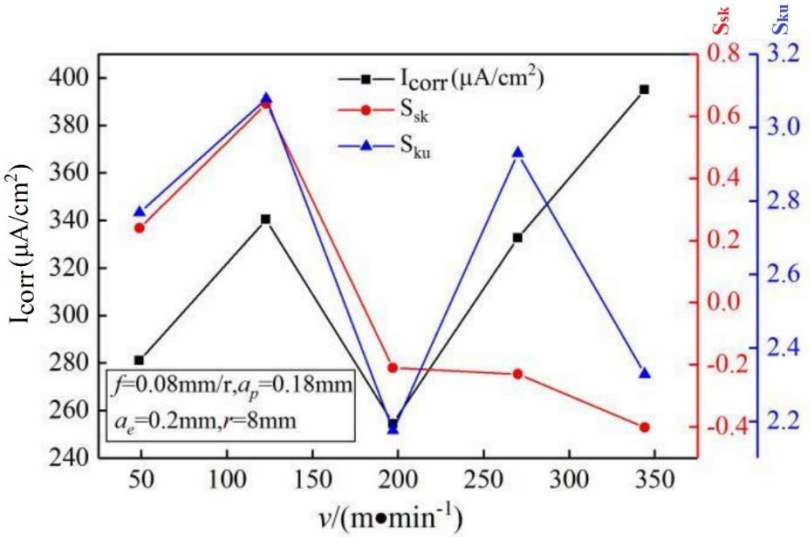

Figure 2. Corrosion current density, skewness and kurtosis under different cutting speed at Cutting depth of 0.18 mm, Row distances of 0.2 mm and Cutter radius of 8 mm

As shown in Figure 2, with an increase in the cutting speed, the corrosion current density initially increased, then decreased and increased again. Such a profile can be attributed to an increase in surface skewness and kurtosis with an increase in cutting speed. This can be related to an increase in the profile peaks on the machined surface, which makes the thickness distribution of the oxide film uneven [20]. Thin oxide layers on the metal surface have a lower polarization resistance and can be broken down by applied correct [21]. When the cutting speed was around 197 m/min, the skewness value was the closest to 0 and the kurtosis value was at its minimum value. As a result, the surface of the sample was very flat and the charge transfer speed was slow. Therefore, a lower corrosion current

density can indicate a better corrosion resistance. As the cutting speed was further increased, plastic deformation, due to thermo-mechanical coupling, occurred on the sample surface, resulting in an increase lateral plastic flow, greater number of deep valleys and more burrs on the machined surface [22, 23]. Under such conditions, the surface amplitude distribution was not found to be uniform resulting in an increase accumulation of solutions in the deep pit area, adsorption of Cl^- ions in the solution, and the destruction of oxide film on the surface, which resulted in a gradual increase in the current density.

As shown in Fig. 3, with the increase in the feed rate, the corrosion current density was found to initially decreased followed by an increase. At feed rate between 0.05 mm/r and 0.15 mm/r, the kurtosis value decreased and the skewness value increased approaching zero with further increase in the feed, which indicates that the surface contour amplitude gradually tends towards a flat surface. When the feed rate was 0.15 mm/r, the surface of sample was very flat, the oxide film on the surface was found to be distributed uniformly and the electric charge was significantly hindered in the transmission process [24]. Furthermore, the corrosion current density reached its minimum value and the machined surface had an increased corrosion-resistance. With further increase of the feed rate, the kurtosis and skewness also increased sharply. It can be attributed to the increase rates in material removal at large feed rates resulting in an increase in the cutting force and eventually, tool tremors [25]. As a result, once more profile peaks and burrs appeared on the surface of Cr12MoV alloy, the corrosion current density gradually increased resulting in a gradual decreased in the corrosion resistance of the material.

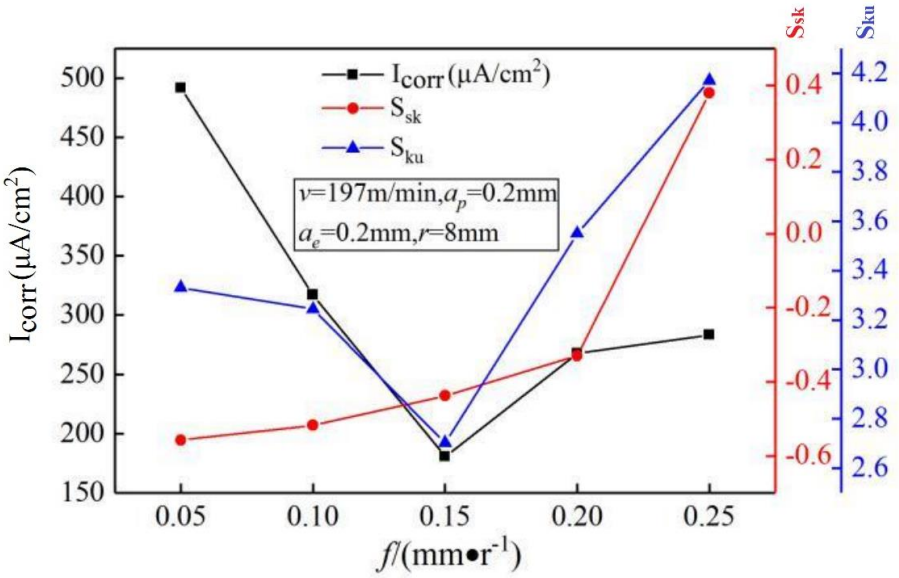

Figure 3. Corrosion current density, skewness and kurtosis under different feed rate at Cutting speed of 197 m/min, Cutting depth of 0.2 mm, Row distances of 0.2 mm and Cutter radius of 8 mm

As a function of cutting depth, the corrosion current density was found to initially decreased followed by an increase (Fig. 4). This behavior could be attributed to the presence of cutting edge of the ball-end milling cutter on both sides which resulted in an increase contact between the cutting edge and the workpiece at low cutting depth [26]. Once the cutting edge extruded the surface of the

workpiece, it was not easy to remove the material, which had increased the surface kurtosis, increased the depth of the surface valley deeper resulting in an uneven distribution of the surface oxide film and making the workpiece more vulnerable to damage [27]. Moreover, it was found that the corrosion current density was high. When the cutting depth was 0.2 mm, the kurtosis value was found to be minimum and the skewness value was found to be close to 0. Which the minimum value of corrosion current density led to the higher corrosion resistance. With the increase in the cutting depth continuously, the material removal rate also increased along with the force of the tool, resulting in machine tool vibration and processing instability [28]. Hence, an increase in the skewness and kurtosis usually resulted in a decrease in the corrosion resistance of the Cr12MoV alloy. However, as the cutting depth changes, the amplitude of skewness and kurtosis fluctuated within a small range, which was smaller than that caused by other factors. It can be concluded that the change in cutting depth had a little effect on the corrosion resistance of the sample [29].

As shown in Fig. 5, with an increase in the cutting row spacing, the corrosion current density initially increased sharply and then decreased. This could be attributed to the lower residual height of the machined surface and the uniform distribution of the surface profile when the row spacing is small [30]. In these conditions, the skewness value is close to 0, the kurtosis value is at its minimum value, the machined surface was smooth, and the Cl^- ions in the solution contacted with the surface evenly, which was the most favorable corrosion resistant conditions observed in the study.

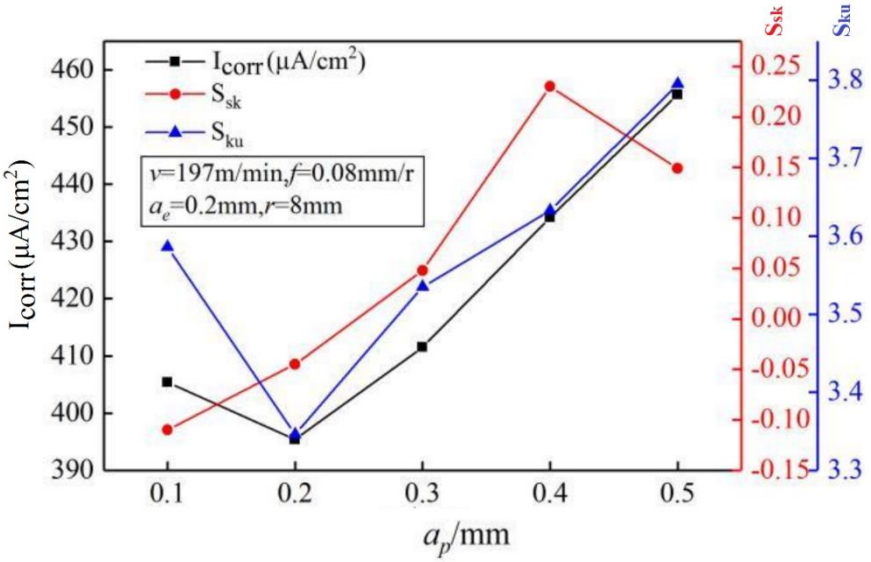

Figure 4. Corrosion current density, skewness and kurtosis under different cutting depth at Cutting speed of 197 m/min, Feed rate of 0.08 mm/r, Row distances of 0.2 mm and Cutter radius of 8 mm

However, as the row spacing increased, the residual height increased, and the residual material left between the milling cutter and the last tool were required to be extruded twice, resulting in plastic deformation. Such a condition made the peak value of the surface higher, the profile peaks more obvious, and reduced the even oxide film distribution on the surface resulting in a damage in the weak areas on the metal surface and sharply increased the corrosion current degree [31].

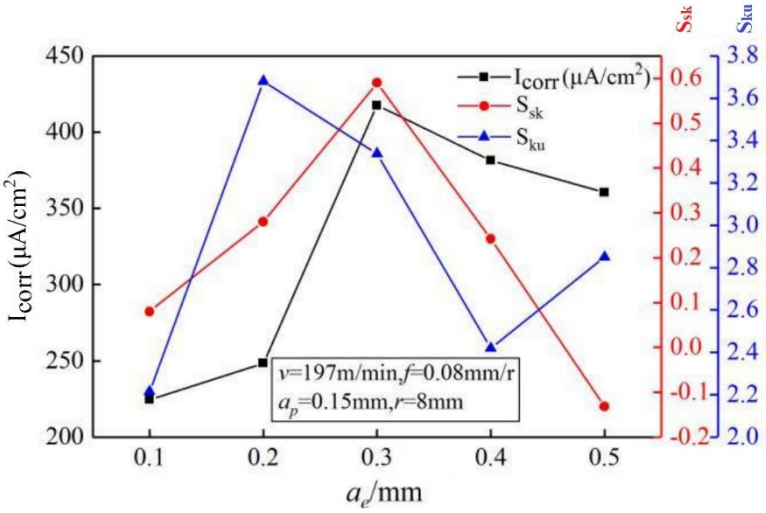

Figure 5. Corrosion current density, skewness and kurtosis under different row spacing at Cutting speed of 197 m/min, Feed rate of 0.08 mm/r, Cutting depth of 0.15 mm and Cutter radius of 8 mm

Once the row spacing were further increased, the extrusion deformation decreased due to an increase in the width of the residual peak. This further resulted in a decreased in the skewness and kurtosis values, and a subsequent decrease in the current density [32]. Therefore, in order to improve the corrosion resistance of the machined surface, it is suggested to adopt a smaller processing row spacing.

As shown in Figure 6, the corrosion current density increased with an increase in the tool radius, and the change amplitude reached a value of 700 μA/cm^2. It was found that a change in the tool radius had a significant effect on the corrosion resistance of the workpiece. When the tool radius was around 5 mm, the deviation value was close to 0, the kurtosis value was very small, the machined surface had better smoothness, the oxide film distribution on the surface was relatively uniform and the corrosion resistance of the workpiece was very good.

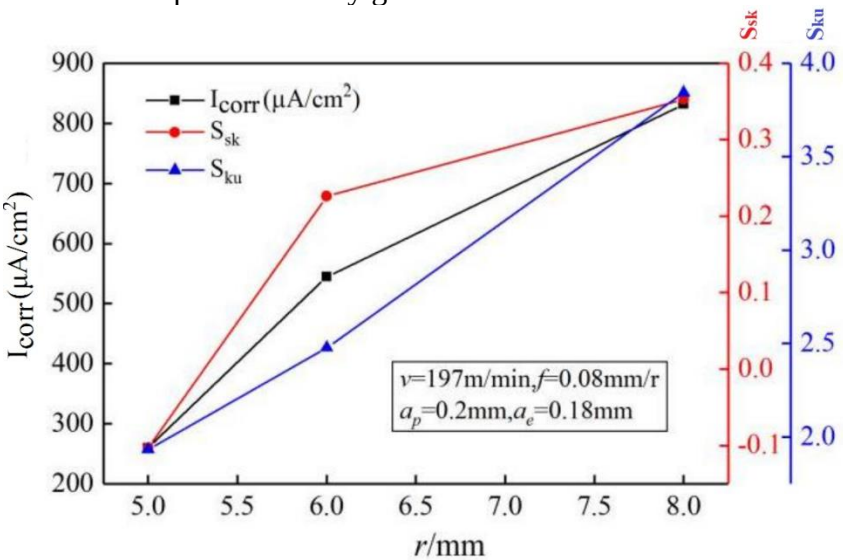

Figure 6. Corrosion current density, skewness and kurtosis under different tool radius at Cutting speed of 197 m/min, Feed rate of 0.08 mm/r, Cutting depth of 0.2 mm and Row distances of 0.18 mm

Thus, it can be concluded that the deviation and kurtosis of the machined surface has a great correlation with the corrosion resistance of the sample. Once the deviation is close to 0 and kurtosis is small, the corrosion resistance of the machined surface was observed to be maximum. As a result, in actual processing, the prediction of corrosion resistance of a workpiece can be achieved by modeling the surface skewness and kurtosis.

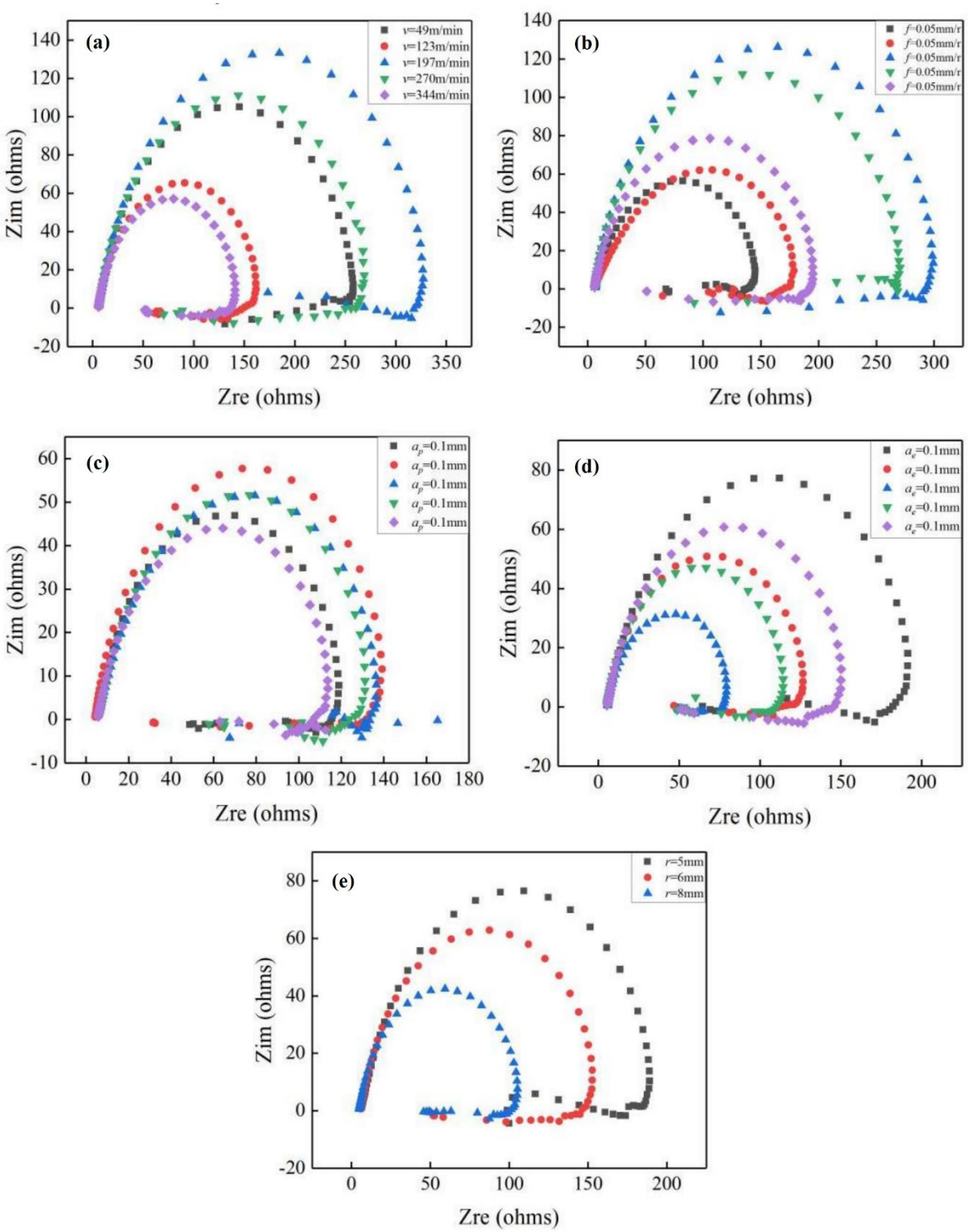

Figure 7. Impedance spectra corresponding to different processing parameters (a) Cutting speed (b) Feed rate (c) Axial cutting depth (d) Row spacing (e) Tool radius at frequency range of 10 000 to 0.01 Hz in electrolyte solution containing 0.1 mol/L HF and 0.3 mol/L HCl

Figure 7 shows the Nyquist plots of the samples exposed to a mixed acid solution under different processing parameters. It can be seen that there are significant differences in the arc radius between the different impedance spectra, but there is a good consistency in the peak shape, i.e., the semi-circular capacitive arc resistance appears in the high-intermediate frequency part of the first quadrant, and the inductive arc appears in the low frequency part of the fourth quadrant [33, 34]. This capacitance resistance arc in the high-intermediate frequency region was caused mainly by the perturbations of the double layer on the electrode surface by the polarization potential and current resulting in a Non-Faradaic process [35]. However, the inductive arc in the low frequency region could be caused by the weakening of the protective property of the oxide film on the metal surface. When the oxide film was perforated, the pitting corrosion was found to enter an expansion stage resulting in a gradual reduction in the corrosion resistance and inductive reactance, which is not reflected in the polarization curve. The impedance spectra show that the oxide film on the surface of the workpiece had been damaged to varying degrees due to corrosion [36]. Although the oxide film on the surface of the material was expected to be dissolved and destroyed, the degree of damage was still found to be varied under different processing parameters. The high-frequency capacitance loop was found to reflect the corrosion resistance of the oxide film on the metal surface [37]. Generally, the larger the diameter of capacitive arc resistance, the greater the resistance of charge transfer making the electrode reactions very difficult to occur.

In order to better understand the corrosion resistance and corrosion mechanism of the oxide film on metal surface, ZsimpWin software was used to fit the equivalent circuit of impedance spectra [38]. The equivalent circuit is shown in Figure 8 and the fitting results are shown in Table 3. The solution resistance (R_s) was found to be affected by the solution concentration and ambient temperature [39]. However, the resistance value was found to have no influence on the fitting results. It can be seen from Table 3 that the R_s fluctuates in a small range while double capacitance (Q) in the corrosive circuit is found to be a constant phase element. The impedance value can be calculated by the following equation [40]:

$$Q = (j\omega)^{-n} / Y_0 \qquad (1)$$

where the Y_0 is the transverse phase angle element constant, n is called diffusion coefficient, $0< n <1$ and R_1 represents charge transfer resistance, which is the main resistance of electrochemical reaction. Table 3 shows that the corrosion resistance of the workpiece expressed by charge transfer resistance is consistent with that expressed by corrosion current density as a function of machine-processing parameters. The fitting results have a higher accuracy and can reflect the actual situation of the workpiece that is undergoing electrochemical corrosion [41]. In Table 3, L and R_{ct} represent the inductance and the resistance of the oxide film on the surface respectively and are parameters that are related to the pitting corrosion.

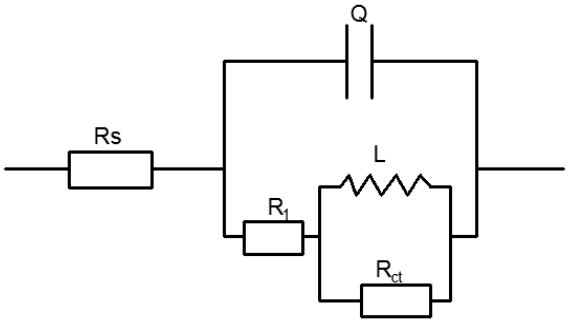

Figure 8. Equivalent circuit diagram

Table 3. Electrochemical Fitting Parameters under Different Processing Parameters according to the equivalent circuit in figure 8.

Machining parameters	R_s /(Ω cm^2)	Y_0/($Ω^{-1}cm^{-1}S^{-n}$)	*n*	R_1 /(Ω cm^2)	L/(Hcm^2)	R_{ct} /(Ω cm^2)
v=49(m/min)	5.867	8.92×10^{-5}	0.8426	182.7	274.8	70.59
v=123(m/min)	6.556	1.098×10^{-4}	0.8568	86.28	118.3	65.74
v=197(m/min)	5.989	8.63×10^{-5}	0.8372	255.1	169.8	72.27
v=270(m/min)	5.93	8.27×10^{-5}	0.8593	145.1	283.4	113.6
v=344(m/min)	5.622	1.202×10^{-4}	0.8641	72.75	130.3	59.34
f=0.05(mm/r)	5.834	1.583×10^{-4}	0.8044	102.9	71.7	39
f=0.1(mm/r)	6.031	2.078×10^{-4}	0.6811	122	67.58	67.58
f=0.15(mm/r)	6.532	7.84×10^{-5}	0.8873	205.8	347.3	84.92
f=0.2(mm/r)	5.876	6.63×10^{-5}	0.833	203.7	293.4	59.57
f=0.25(mm/r)	5.753	9.61×10^{-5}	0.8534	125.7	125.7	62.77
a_p=0.1(mm)	5.512	1.501×10^{-4}	0.8456	77.79	109.3	45.65
a_p=0.2(mm)	4.32	1.332×10^{-4}	0.8616	93.15	92.98	54.5
a_p=0.3(mm)	5.671	1.968×10^{-4}	0.7729	66.18	6.018	20.42
a_p=0.4(mm)	6.192	1.49×10^{-4}	0.8293	65.1	81.93	49.12
a_p=0.5(mm)	5.604	1.998×10^{-4}	0.8131	62.3	9.25	20.56
a_e=0.1(mm)	6.29	1.142×10^{-4}	0.8428	117.4	136	66.86
a_e=0.2(mm)	5.702	1.271×10^{-4}	0.8574	67.41	103.5	50.76
a_e=0.3(mm)	5.629	1.934×10^{-4}	0.8447	49.64	16.39	25.17
a_e=0.4(mm)	5.29	1.369×10^{-4}	0.8781	61.15	67.35	45.28
a_e=0.5(mm)	5.675	1.054×10^{-4}	0.863	84.19	123.2	56.76
r=5(mm)	6.559	1.025×10^{-4}	0.8335	131.3	102	52.64
r=6(mm)	6.032	1.392×10^{-4}	0.8574	81.78	135	62.55
r=8(mm)	4.845	1.383×10^{-4}	0.9619	54.68	58.93	43.37

The surface morphology of the sample after electrochemical corrosion is shown in Figure 9a. A large number of corrosion products seem to be accumulated on the corroded surface, and the oxide film on the surface has been completely destroyed (resulting in a rough surface). The volume of corrosion products had increased resulting in corrosion cracks on the surface of the workpiece.

The energy spectrum used for scanning the sample surface after corrosion is shown in Figure 9b. The new elements were found to be O, F and Cl. This showed that there are a lot of C element accumulation and more metal oxides in the corrosion products, as can be evident by the presence of F-element in the solution [42]. The results indicate that there were more corrosion residues in the area,

i.e., the corrosion degree was relatively heavy. The composition of Cl ions were present in the corrosion products, although they were relatively low. During the corrosion process, Cl^- was found to be easily adsorbed and aggregated at the incomplete oxide film or the uneven micro-structure on the machined surface, resulting in a thinning and rupture of the oxide film, which further resulted in a direct contact of the metal on the surface of the workpiece with the corrosive solution [43].

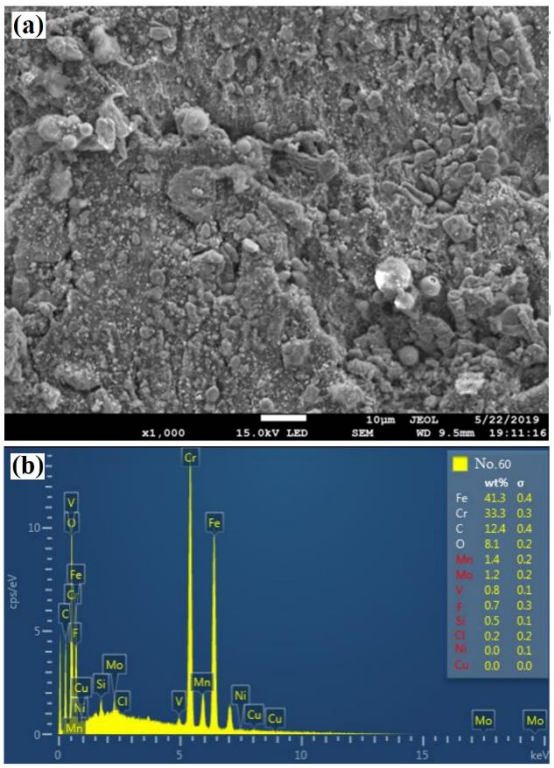

Figure 9. (a) Surface Morphology of Electrochemical Corrosion (b) Energy Spectrum of Corroded Surface of Cr12MoV die steel in electrolyte solution containing 0.1 mol/L HF and 0.3 mol/L HCl

4. CONCLUSIONS

The corrosion resistance of Cr12MoV die steel was found to be closely related to the skewness and kurtosis of the machined surface. When the skewness was close to 0, the kurtosis of the peaks were found to be smaller resulting in an increase in corrosion resistance of the machined surface. Under processing conditions of v=197m/min, f=0.15mm/r, a_p=0.2mm, a_e=0.1mm, r=5mm, the machined surface showed better corrosion resistance. Among these conditions, the change of cutting depth had little effect on the corrosion resistance of the material surface. However, smaller path interval spacing and lower tool radius were found to increase the corrosion resistance of the workpiece, and the change in tool radius had a significant impact on the corrosion resistance of the workpiece. The shape of the polarization curves and impedance spectra of samples at different processing parameters were found to be comparable to each other. By varying the processing parameters, the corrosion resistance of the workpiece (charge transfer resistance) was consistent with the corrosion current

density. These results indicate that the fitting result of equivalent circuit had a higher accuracy which can be related to the actual situation of a workpiece during electrochemical corrosion. During the electrochemical corrosion process, the surface oxide during the pitting induction period had a higher inductive reactance. The SEM results revealed that the corrosion products were found to significantly accumulate on the surface of the workpiece. The EDS analysis indicated that there were a lot of C element accumulation and more metal oxides in the corrosion products, as can be evidenced by the presence of F element in the solution. The study also showed that the aggregation of Cl^- ions will accelerate the destruction of the oxide film on the surface.

ACKNOWLEDGEMENTS
This work was supported by National Natural Science Foundation of China (51675231) and the Fundamental Research Funds for the heilongjiang Universities（2016-KYYWF-0551).

References

1. J. Qiu, X. Li, X. Ma, J. Lin and J. Tong, *Zhongguo Jixie Gongcheng(China Mechanical Engineering)*, 23 (2012) 1555.
2. P. Forsyth, *Materials science and technology*, 14 (1998) 151.
3. N. Naderi, M. Hashim and J. Rouhi, *International Journal of Electrochemical Science*, 7 (2012) 8481.
4. S. Zhang, J. Zhang, H.-l. Zheng and C.-y. Wu, *Corrosion and Protection*, 33 (2012) 1.
5. C.A. de Oliveira Junior, A.E. Diniz and R. Bertazzoli, *Journal of the Brazilian Society of Mechanical Sciences and Engineering*, 36 (2014) 775.
6. F. Husairi, J. Rouhi, K. Eswar, C.R. Ooi, M. Rusop and S. Abdullah, *Sensors and Actuators A: Physical*, 236 (2015) 11.
7. R. Zhang, Y. Wan, C. Li and Z. Liu, *Tool Engineering*, 45 (2011) 12.
8. T. Liptáková, A. Alaskari, L. Trško and S. Dundeková, *Transactions of FAMENA*, 41 (2017) 81.
9. S. Zhang, C. Wu, C. Zhang, M. Guan and J. Tan, *Optics & Laser Technology*, 84 (2016) 23.
10. S. Chen, J. Huang, J. Xia, X. Zhao and S. Lin, *Journal of Materials Processing Technology*, 222 (2015) 43.
11. H. Rao, S. Giet, K. Yang, X. Wu and C.H. Davies, *Materials & Design*, 109 (2016) 334.
12. B. MENG, W.-l. GUO and Y. JIANG, *Materials for Mechanical Engineering*, 8 (2008) 1.
13. Y. Wang, G. Cheng, W. Wu, Q. Qiao, Y. Li and X. Li, *Applied Surface Science*, 349 (2015)
14. M. Alimanesh, J. Rouhi and Z. Hassan, *Ceramics International*, 42 (2016) 5136.
15. J. Du, K. Xiang, L. Zhao, X. Lan, P. Liu and Y. Liu, *International Journal of Electrochemical Science*, 14 (2019) 8919.
16. Y.-j. Chu, B.-x. Hao, P. Liu and Y.-b. Zhang, *Materials Research*, 22 (2019) e20190068.
17. G. Krolczyk, J. Krolczyk, R. Maruda, S. Legutko and M. Tomaszewski, *Measurement*, 88 (2016) 176.
18. F. Rivas-Esquivel, G. Brisard, R. Ortega-Borges, G. Trejo and Y. Meas, *International Journal of Electrochemical Science*, 12 (2017) 2026.
19. C. Li, S. Hu, L. Yang, J. Fan, Z. Yao, Y. Zhang, G. Shao and J. Hu, *Chemistry–An Asian Journal*, 10 (2015) 2733.
20. L. Yang, G. Yi, Y. Hou, H. Cheng, X. Luo, S.G. Pavlostathis, S. Luo and A. Wang, *Biosensors and Bioelectronics*, 141 (2019) 111444.
21. D.Y. Hwang, Y.M. Kim, D.-Y. Park, B. Yoo and D.H. Shin, *Electrochimica Acta*, 54 (2009) 5479.

22. T. Mabrouki and J.-F. Rigal, *Journal of Materials Processing Technology*, 176 (2006) 214.
23. R. Dalvand, S. Mahmud and J. Rouhi, *Materials Letters*, 160 (2015) 444.
24. P. Shao, X. Duan, J. Xu, J. Tian, W. Shi, S. Gao, M. Xu, F. Cui and S. Wang, *Journal of hazardous materials*, 322 (2017) 532.
25. J.F.G.d. Oliveira, E.J.d. Silva, C. Guo and F. Hashimoto, *CIRP annals*, 58 (2009) 663.
26. M. Luo, H. Luo, D. Zhang and K. Tang, *Journal of Materials Processing Technology*, 252 (2018) 105.
27. P. Shao, L. Ding, J. Luo, Y. Luo, D. You, Q. Zhang and X. Luo, *ACS applied materials & interfaces*, 11 (2019) 29736.
28. E. Ozturk, A. Comak and E. Budak, *Journal of Sound and Vibration*, 360 (2016) 17.
29. M. Uddin, H. Rosman, C. Hall and P. Murphy, *The International Journal of Advanced Manufacturing Technology*, 90 (2017) 2095.
30. X. He, F. Deng, T. Shen, L. Yang, D. Chen, J. Luo, X. Luo, X. Min and F. Wang, *Journal of colloid and interface science*, 539 (2019) 223.
31. K. Khaled and N. Al-Mobarak, *International Journal of Electrochemical Science*, 7 (2012) 1045.
32. G. Siracusano, R. Tomasello, M. d'Aquino, V. Puliafito, A. Giordano, B. Azzerboni, P. Braganca, G. Finocchio and M. Carpentieri, *IEEE Transactions on Magnetics*, 54 (2018) 1.
33. D. Yuan, C. Zhang, S. Tang, X. Li, J. Tang, Y. Rao, Z. Wang and Q. Zhang, *Water research*, 163 (2019) 114861.
34. J. Rouhi, S. Mahmud, S.D. Hutagalung and S. Kakooei, *Journal of Micro/Nanolithography, MEMS, and MOEMS*, 10 (2011) 043002.
35. M. Łukaszewski, M. Soszko and A. Czerwiński, *International Journal of Electrochemical Science*, 11 (2016) 4442.
36. H. Chen, S. Zhang, Z. Zhao, M. Liu and Q. Zhang, *Progress in Chemistry*, 31 (2019) 571.
37. G. Tranchida, M. Clesi, F. Di Franco, F. Di Quarto and M. Santamaria, *Electrochimica Acta*, 273 (2018) 412.
38. S.B. Aoun, M. Bouklah, K. Khaled and B. Hammouti, *International Journal of Electrochemical Science*, 11 (2016) 7343.
39. F. Husairi, J. Rouhi, K. Eswar, A. Zainurul, M. Rusop and S. Abdullah, *Applied Physics A*, 116 (2014) 2119.
40. A. Ghazoui, N. Benchat, F. El-Hajjaji, M. Taleb, Z. Rais, R. Saddik, A. Elaatiaoui and B. Hammouti, *Journal of Alloys and Compounds*, 693 (2017) 510.
41. S. Tang, N. Li, D. Yuan, J. Tang, X. Li, C. Zhang and Y. Rao, *Chemosphere*, 234 (2019) 658.
42. P. Shao, J. Tian, F. Yang, X. Duan, S. Gao, W. Shi, X. Luo, F. Cui, S. Luo and S. Wang, *Advanced Functional Materials*, 28 (2018) 1705295.
43. P. Shao, J. Tian, X. Duan, Y. Yang, W. Shi, X. Luo, F. Cui, S. Luo and S. Wang, *Chemical Engineering Journal*, 359 (2019) 79.